

eSampling: Rethinking Sampling with Energy Harvesting

Neha Jain^{*†}, Bhawna Tiwari, Anubha Gupta[†], Vivek Ashok Bohara^{*} and Pydi Ganga Bahubalindrani[‡]

^{*}Wirocomm Research Lab, [†]Signal processing and Bio-medical Imaging Lab (SBILab)

Department of Electronics and Communication Engineering,

Indraprastha Institute of Information Technology-Delhi (IIIT-D), New Delhi, India

[‡]Indian Institute of Technology, Goa, India

Email:nehaj@iiitd.ac.in, bhawnat@iiitd.ac.in, anubha@iiitd.ac.in, vivek.b@iiitd.ac.in and bpganga@iitgoa.ac.in

Abstract—In general, real world signals are analog in nature. To capture these signals for further processing, or transmission, signals are converted into digital bits using analog-to-digital converter (ADC). In this conversion, a good amount of signal energy is wasted because signal that is captured within the sampling duration is utilized, while rest of the signal waveform is discarded. In this context, this paper revisits the sampling process and proposes to utilize this discarded signal for energy harvesting, naming the method as *eSampling*, i.e., sampling with energy harvesting. The proposed idea of *eSampling* is demonstrated via modifying the circuitry of the hold phase of ADC. The system is designed using standard Complementary Metal Oxide Semiconductor (CMOS) 65 nm technology and simulations are performed on Cadence Virtuoso platform with input signal at different frequencies (100 Hz and 40 MHz). These results show that 10% of the sampling period is sufficient to sample the input analog signal, while the remaining 90% can be used for harvesting the energy from the input analog signal. In order to validate *eSampling* for practical scenarios, results with hardware setup have also been added.

Index Terms—Energy harvesting, Sampling, Sampling period and Analog-to-digital converter

I. INTRODUCTION

Energy harvesting (EH) via ambient sources has become an important area of research due to the advent of low power [1], [2] and small form-factor devices [3], [4]. Small form factor has not only led to reduction in size of electronic devices, but also enhanced its functionality. This has also led to plethora of wearable devices that has replaced most of the functionalities of portable devices. For instance, smart watches have replaced some of the functionalities of smart phones. Further, the advancement in low power microelectronics technology has reduced the power consumption of devices by a considerable amount and hence, devices can be operated by harvesting the energy from ambient sources. Energy harvesting can either increase the lifetime of the device or can ensure a battery-free system [5]. Similarly, in case of wireless sensor networks (WSNs), battery-free sensors can eliminate the difficulties of replacing or recharging the batteries at remotely located sensors [6]–[8]. EH also finds applications in toxic environments, medical body area networks (MBANs), and body area networks (BANs) [9]–[11], where replacing or recharging batteries is an arduous task.

Energy can be harvested either from human activities such as walking, jogging, and cycling [12], [13] or from environmental sources such as solar [14], [15], wind [16], thermal [17] and mechanical pressure etc. [18]. Recently, harvesting the energy from radio frequency (RF) signals has gained a lot of popularity over other energy sources [19]. The foremost reason for the same is that RF signals, being harvested, are abundant in the humanized environment, whereas solar/wind resources are not perennially available. Furthermore, RF signals contain both information as well as energy and hence, an energy constrained receiver can decode the information as well as harvest the energy. This method is known as simultaneous information and power transfer (SWIPT). The two realistic protocols for SWIPT, namely, time switching (TS) and power splitting (PS) [20], [21] affect the system performance in order to harvest the energy. However, the phrase ‘energy harvesting’ refers to the process of converting discarded/wasted/unused energy into useful electrical energy for fulfilling the energy requirements, for instance, solar EH. Thus, energy should be harvested from the discarded signals without degrading system performance.

In this paper, we propose a novel method for energy harvesting termed as *eSampling*, where *e* signifies the process of energy harvesting. *eSampling* has been proposed for harvesting the unused/discarded signal energy during the sampling process of an analog-to-digital converter (ADC). Since most of the real signals are analog in nature, to capture and store the data, these are converted into equivalent digital bits by using an ADC. An ADC consists of two processes, namely *sampling* and *quantization*. Sampling converts the input analog signal into discrete samples, while quantization converts the discrete samples into digital bits. Typically, a sample and hold (S/H) circuit is used to sample the input analog signal in an ADC. The S/H circuit consists of two phases, *acquisition phase* and *hold phase*. In acquisition phase, the S/H circuit tracks the input analog signal. The sampled value captured in the acquisition phase is converted into digital bits during hold phase. Therefore, during sampling process of an ADC, the input signal is processed only for a small fraction of time (acquisition phase) and neglected/discarded for the remaining time interval (hold phase). Hence, a method *eSampling* is proposed which modifies the hold phase of the sampling

process to harvest the energy from the input signal. To the best of our knowledge, no such work has been reported till date which harvests the input signal energy during the sampling process without degrading the performance of an ADC or any another block in the system.

A. Related work

In literature, methods have been proposed for harvesting energy from discarded signals [22], [23]. For example, a method has been proposed for harvesting energy during modulation and filtration in [22]. Since a part of signal energy is often discarded or lost during modulation, this can be harvested to generate electrical power. Likewise, filtering also discards some part of the signal in the process of accomplishing desirable task. Signal portion discarded during filtering can be utilized to harvest energy. Similarly, signal energy has been harvested from the redundant portion (i.e. the cyclic prefix) in Orthogonal Frequency Division Multiple Access (OFDMA) system in [23].

The method *eSampling* has worldwide applications, since real signals are analog in nature and most of the existing systems are energy constrained. For example, the proposed method can be directly utilized in WSNs because the sensor nodes are energy constrained nodes and are typically powered by batteries with a limited lifetime [24]. Therefore, energy harvesting systems can be employed to supplement the lifetime of the battery. Most of the recent work focuses on developing an effective energy management solution [25]–[28] because even though additional energy can be harvested from the external environment, it remains a limited resource, and hence should be consumed wisely. Effective energy management relies on re-designing of circuit to harvest maximum available energy [25], [26] and also on re-designing of network which includes various opportunistic transmission strategies and routing algorithms to reduce the energy consumption [27], [28]. On the other hand, the current work proposes an entirely different approach and provides an alternative form of energy harvesting that is carried out during the sampling of its own sensed analog signal. Generally, sensor nodes generate analog signals corresponding to the sensed parameters that are digitized using ADC and are transmitted to the Fusion center [8], [24]. The generated analog signals at sensor nodes have a good amount of energy that was wasted earlier. This energy can be harvested by using the proposed *eSampling* method. Therefore, self-sustainable wireless sensor nodes can be fabricated that can charge themselves from their own sensed parameter without using any dedicated energy harvesting source. Similar to above, *eSampling* method will find tremendous utility in wireless body area network (WBAN) because sensor devices are generally autonomous and implanted inside the body, where batteries are irreplaceable [29]. Further, the proposed *eSampling* method can be applied to numerous industrial application scenarios including but not limited to radar, wireless communication [30]–[32], vehicular networks [33] and Internet of things [25]–[28]. In future, energy constrained devices or circuits involving sampling process at some stage may like to replace the conventional

sampling with *eSampling* with re-design of the associated circuitry.

Rest of the paper is organized as follows: Section II describes the proposed *eSampling* method, Section III reports the simulation model designed for *eSampling*, Section IV discusses simulation results for the validation of the proposed method and Section V provides the real time validation of *eSampling* using hardware setup. Finally, conclusions are drawn in section VI.

II. PROPOSED *eSampling* METHOD

A. Overview

Consider Fig. 1a) and b) that describe the acquisition and hold phase of the sampling process, respectively controlled by a common sampling clock (*Clk*). The acquisition phase is the duration for which S/H switch is connected to capacitor C_h to track the input analog signal. Once the acquisition phase is over, the hold phase starts. In this phase, the S/H switch is open or disconnected from C_h as shown in Fig. 1b) such that C_h can hold the sampled value acquired in the acquisition phase. This signal value is converted into digital bits using the quantization process. This is to be noted that the discarded input signal during the hold phase contains a considerable amount of energy that can be harvested. In this work, we propose an alternative phase, henceforth called as EH phase, during which the switch will be connected to another capacitor C_{EH} to store the energy as shown in Fig. 1c). This phase can be seen as the modified version of the hold phase of the conventional ADC. It should be noted that the modified hold phase with the EH phase does not impact the functionality of the conventional ADC circuit.

Consider an input analog signal with maximum signal frequency f_m sampled at Nyquist sampling rate. Hence, the sampling period is given as $T_s = \frac{1}{f_s} \leq \frac{1}{2f_m}$, where f_s is the sampling frequency. The sampling period is given by

$$T_s = T_{aq} + T_h, \quad (1)$$

where T_{aq} is the acquisition time or the time allocated to the acquisition phase as shown in Fig. 1a). It is defined as the minimum time required for C_h to charge itself to the full input signal voltage. T_h is the hold time during which the input analog signal is disconnected from the ADC and the sampled value obtained across C_h is converted by ADC into corresponding digital bits as shown in Fig. 1b). Since the input analog signal is not processed during T_h , it can be harvested to recharge the batteries or to drive other on-chip circuits.

B. *eSampling* System Model

Fig. 2(a) presents the block diagram of *eSampling* system with input signal ($V_{in}(t)$). It comprises of two branches: ADC branch and EH branch. A differential Successive-Approximation Register (SAR) ADC has been employed in the ADC branch of the system that comprises of a sampling switch ($S1$), a voltage comparator, a digital-to-analog converter (DAC), and a SAR logic. On the other hand, EH branch consists of a switch $S2$, a rectifier, and an energy storage capacitor (C_{EH}). The voltage across the capacitor

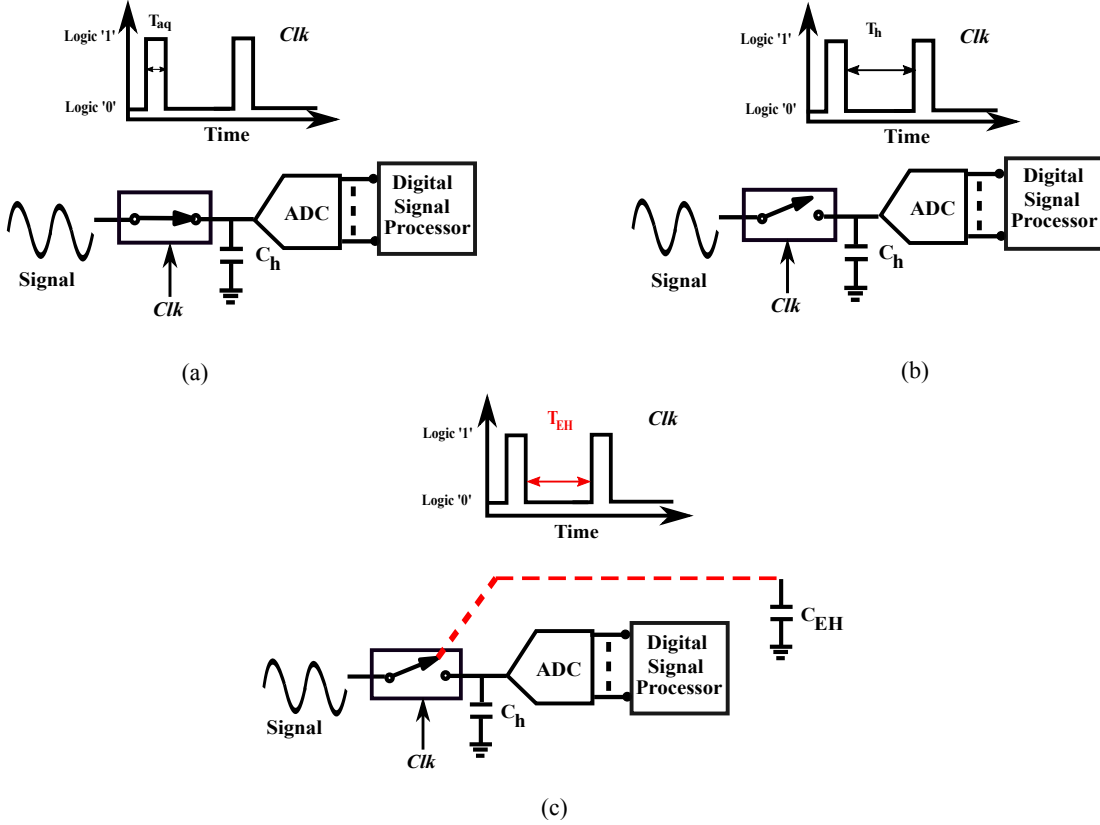


Fig. 1. Typical data acquisition system with different phases (a) Acquisition phase (b) Hold phase and (c) Energy harvesting phase.

is denoted as V_{EH} . Switches $S1$ and $S2$ of the model are controlled by Clk as shown in Fig. 2(b). The operation of $eSampling$ system is divided in two phases:

Acquisition Phase ($S1$ is ON and $S2$ is OFF): The time period of this phase is equal to T_{aq} . The equivalent block diagram is shown in Fig. 2(c). The functioning of both ADC and EH branch in acquisition phase is described below.

- ADC branch: Input analog signal from the surrounding or preceding blocks is sampled onto the DAC capacitors of SAR ADC [34].
- EH branch: It is isolated from the signal source ($V_{in}(t)$).

Energy harvesting (EH) Phase ($S1$ is OFF and $S2$ is ON): The time period of this phase is equal to T_h . The equivalent block diagram is shown in Fig. 2(d). The functioning of ADC and EH branch in EH phase is explained below.

- ADC branch: SAR ADC converts the sampled signal into equivalent digital bits using a quantizer.
- EH branch: The input analog signal is rectified to store the maximum amplitude of the signal on capacitor C_{EH} . However, due to non-idealities associated with the rectifier and switches, certain voltage drop is experienced. Hence, the maximum voltage on C_{EH} is given by

$$V_{EH} = \eta_v V_M, \quad (2)$$

where V_M is the maximum amplitude of the input signal $V_{in}(t)$ and $0 < \eta_v \leq 1$ is the efficiency of the EH

branch. Further, the maximum time that can be assigned for harvesting the input signal energy is given by using (1) as below:

$$T_{EH} = T_s - T_{aq}. \quad (3)$$

The amount of energy harvested/stored from the input analog signal can be calculated as

$$E_h = \frac{1}{2} C_{EH} V_{EH}^2, \quad (4)$$

The conversion efficiency, i.e., the percentage of energy harvested from the input signal until C_{EH} attains the steady state is given by

$$\begin{aligned} \eta_e &= \frac{E_h}{E_{in}} \\ &= \frac{C_{EH} V_{EH}^2}{2 P_{in} T_{C_{EH}}}, \end{aligned} \quad (5)$$

where P_{in} is the root mean square (rms) power of the input signal $V_{in}(t)$ and $T_{C_{EH}}$ denotes the time taken by energy harvesting capacitor (C_{EH}) to charge up to steady state voltage, i.e., V_{EH} .

III. SIMULATION MODEL

In order to demonstrate the proposed idea, a system model is designed using standard 65 nm Complementary Metal Oxide Semiconductor (CMOS) technology. Design details of all sub-blocks in the system model are described below.

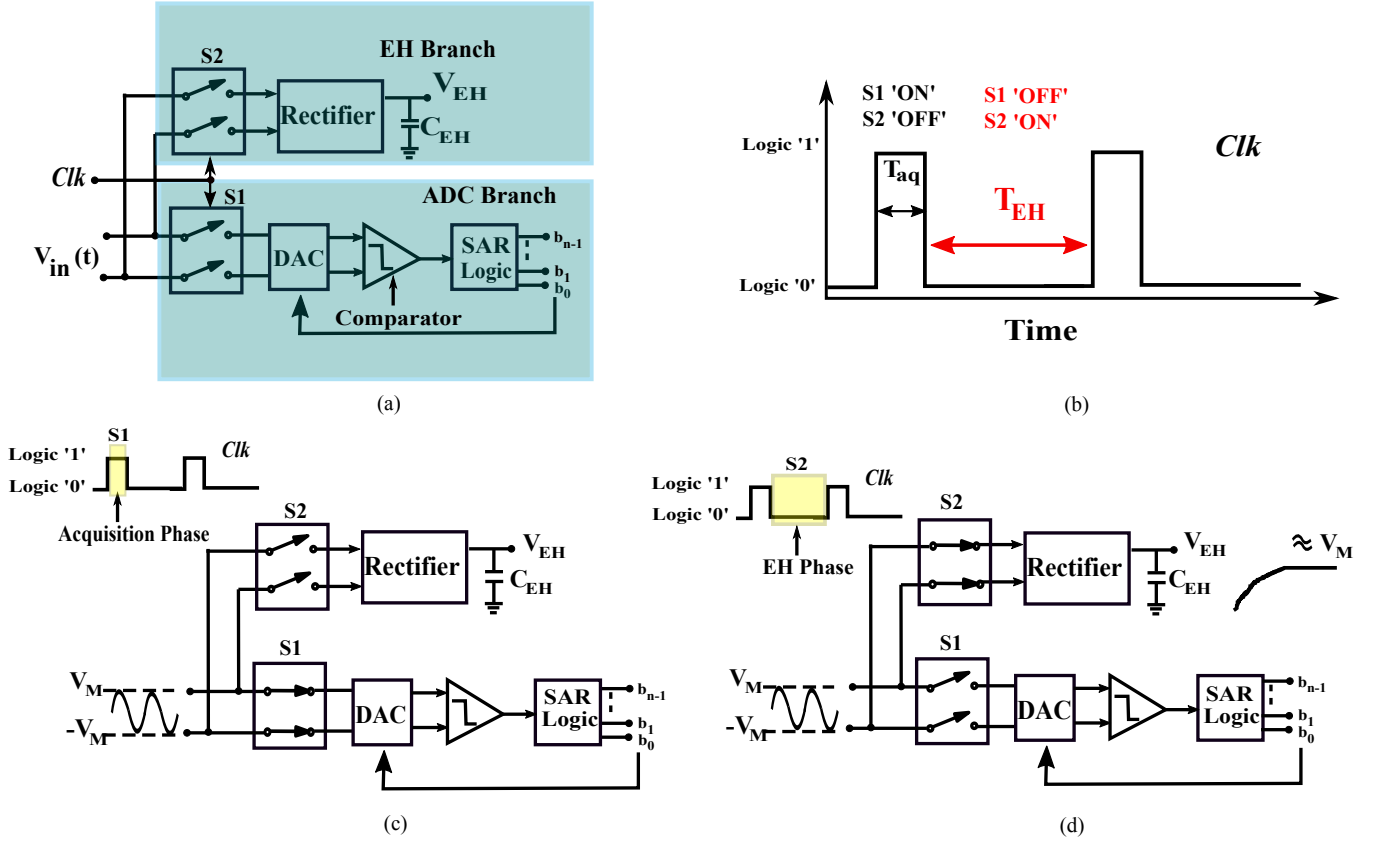


Fig. 2. Block diagram of (a) *eSampling* system model, (b) Sampling clock, (c) Acquisition phase and (d) EH phase.

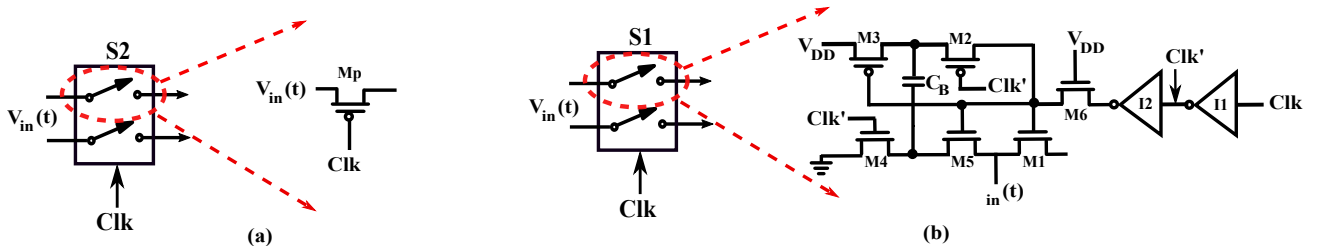


Fig. 3. Circuit Diagram of (a) p-channel pass transistor switch used as $S2$ in system model, (b) Bootstrapped switch used as $S1$ in system model.

1) *Switches*: Switches $S1$ and $S2$ follow differential implementation and are realized using two different switch topology. $S1$ is implemented using n-channel MOS (NMOS) bootstrapped switch [35], while $S2$ is implemented using p-channel MOS (PMOS) pass transistors. Both switches are controlled by Clk .

Switch $S2$ is implemented using two PMOS transistors as shown in Fig. 3(a). The PMOS transistor turns ON and passes the input signal ($V_{in}(t)$) when Clk is at logic '0'. However, it turns OFF and isolates the input signal from the next block when Clk is at logic '1'. PMOS transistors are used instead of NMOS because PMOS transistors pass the logic '1' (high voltage) without experiencing the voltage drop.

The on-resistance, R_{ON} of a pass transistor Mp is given by [36]

$$R_{ON} = \frac{1}{\mu C_{ox} \frac{W}{L} (|V_{GS}| - |V_{TH}|)}, \quad (6)$$

where μ is the mobility, C_{ox} is the oxide capacitance, $\frac{W}{L}$ is the aspect ratio, V_{GS} is the gate-to-source voltage, and V_{TH} is the threshold voltage of the transistor. V_{GS} of the pass transistor varies with time according to the input signal $V_{in}(t)$ and hence, R_{ON} will also vary as given in (6). The variation in the R_{ON} introduces non-linear distortion at the output of ADC and hence, bootstrapped switch is generally used for ADC. The bootstrap switch can typically ensure constant R_{ON} [35].

Switch $S1$ is implemented using two NMOS single-ended bootstrapped switches as shown in Fig. 3(b). In order to ensure a nearly constant R_{ON} , the gate of transistor $M1$ is bootstrapped using two PMOS transistors $M2$ and $M3$, three NMOS transistors $M4$, $M5$ and $M6$, and one capacitor C_B [35]. Two CMOS inverters $I1$ and $I2$ are also employed in the structure to generate required clock signals for proper operation of the switch.

2) *ADC*: The architecture of SAR ADC is implemented using a sampling switch $S1$, voltage comparator, SAR logic, and DAC. Switch $S1$ is a bootstrap switch as explained above. A two stage voltage comparator is implemented, where the first stage is a dynamic pre-amplifier and second stage is a latch [37]. Furthermore, SAR logic is implemented using two arrays of shift registers that operate in serial-in-serial-out and parallel-in-parallel-out modes [38]. The ADC operates asynchronously, hence the clock pulses for comparator and SAR logic are generated internally from Clk using clock generation logic [38]. In addition, binary-weighted capacitive DAC is used in the ADC. The capacitive DAC is implemented using merge capacitor switching (MCS) scheme [34] because it eliminates the most significant bit (MSB) capacitor compared to conventional design [39] and hence, reduces the total capacitance of the DAC (C_{DAC}) by half. It should be noted that C_{DAC} of SAR ADC mimics C_h (Fig. 1). By reducing C_{DAC} , T_{aq} of the ADC can be reduced, because T_{aq} is defined as [36]

$$T_{aq} = R_{ON}^{S1} C_{DAC}, \quad (7)$$

where R_{ON}^{S1} is the on-resistance of $S1$ switch. Further, C_{DAC} for n -bit SAR ADC is defined as

$$C_{DAC} = \left(1 + \sum_{i=0}^{n-2} 2^i \right) C_u, \quad (8)$$

where C_u is the unit capacitor of the DAC array. *eSampling* demands low value of T_{aq} so that more time could be allocated for harvesting the input signal energy (3). It should be noted that to further reduce T_{aq} , C_{DAC} and R_{ON}^{S1} should be reduced as evident from (7). Reducing R_{ON}^{S1} demands wider transistors, which in turn increases the device capacitance and thus, reduces the operating speed of the ADC. In addition, wider devices leads to charge injection problem, which degrades the SNR of the ADC and hence, the performance of the ADC is compromised. On the other hand, employing small values for C_{DAC} results in mismatch issues and sampling noise, which degrade the ADC conversion accuracy. These issues demand the T_{aq} to be large enough such that the ADC performance is not compromised. A large T_{aq} will reduce time available for the energy harvesting, T_{EH} . As a consequence, there is trade-off between T_{EH} and T_{aq} .

3) *Rectifier*: A full wave rectifier has been employed in the simulation model as shown in Fig. 4. Due to inherent threshold voltage drop in NMOS transistor, the rectifier is implemented using PMOS (p-type MOS) transistors. The two PMOS transistors have been connected in a cross-coupled fashion as shown in Fig. 4. It should be noted that in this circuit, a negative to positive transition at point **A** results in positive to negative transition at point **B**, and hence, $M1$ is ON and $M2$ is OFF. While in vice-versa condition, $M1$ is OFF and $M2$ is ON. Therefore, a full wave rectification can be observed at the output.

IV. SIMULATION RESULTS AND DISCUSSIONS

A complete schematic of the *eSampling* model has been created in Cadence Virtuoso platform. Schematic simulation

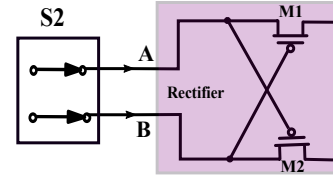


Fig. 4. Circuit Diagram of Rectifier.

uses mathematical models, which help us to authenticate the behavior of *eSampling*. However, schematic simulations exclude the effect of parasitic capacitance and resistance associated with the connecting wires and devices employed in the system model. Therefore, post-layout simulations have been also performed to ensure similar performance of the model when fabricated to work in real world environment. Since the focus of the paper is to harvest maximum energy from the input signal without effecting the performance of ADC, post-layout simulations were carried out for switch $S1$ and EH branch. Layouts of these blocks are presented in Fig. 5. It should be noted that for obtaining the desirable performance of n -bit ADC, the output signal-to-noise and distortion ratio (SNDR) of $S1$ should be greater than $6.02n + 1.76$ dB [36].

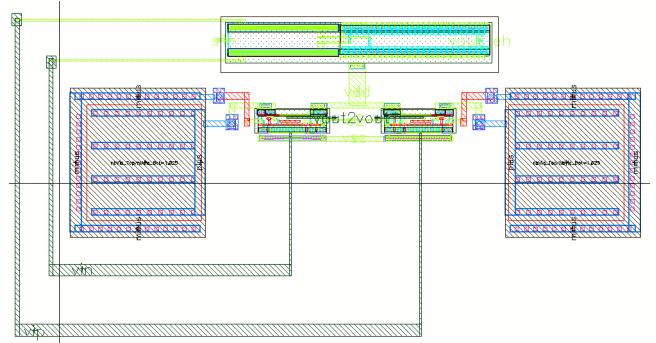


Fig. 5. Layout of the *eSampling* model.

To demonstrate the efficiency of the proposed idea of energy harvesting along with sampling, an 8-bit SAR ADC has been used in the ADC branch of the *eSampling* system. In addition, to cover a wide range of applications, *eSampling* system has been simulated for both low (KHz) as well as high (MHz) input signal frequencies. During simulation, the acquisition time is chosen to be 10% of the total sampling period, i.e., $T_{aq} = 0.1 T_s$ such that 90% of the sampling time can be allocated for energy harvesting, i.e., $T_{EH} \approx 0.9 T_s$.

A. Low-frequency Simulation of *eSampling* System

Low frequency simulations are performed at a sampling frequency ($\frac{1}{T_s}$) of 10 KHz. The frequency of the input signal is calculated using coherent sampling principle and following the Nyquist rule. A sinusoidal signal with amplitude varying from -0.4 V to 0.4 V is selected as an input with an input rms power of $27.7 \mu\text{W}$ for a source impedance of 50 ohm.

A SAR ADC has been designed to operate at $T_{aq} = 0.1 T_s = 10 \mu\text{s}$ with $C_u = 12 \text{ nF}$. From schematic

simulations, the output SNDR of $S1$ is around 65 dB. The FFT plot of the reconstructed signal is presented in Fig. 6, which shows SNDR of 49 dB and ENOB (equivalent number of bits) equals to 7.85 bits for an 8-bit ADC that implies no loss of bits. In addition, from post-layout simulations, the obtained output SNDR of $S1$ is around 62 dB, which is greater than $6.02n + 1.76$ dB. Therefore, as mentioned above, it can drive an 8-bit SAR ADC.

Simulation results of EH branch is presented in Fig. 7. It is observed that when Clk is 'logic 0' (during T_{EH} time period), the two PMOS transistors defining the $S2$ switch track the input analog signal $V_{in}(t)$ that will be the input of the rectifier V_{in}^{rec} . Rectifier rectifies V_{in}^{rec} to provide a DC output voltage V_{EH} . Consider Fig. 8 for both schematic and post-layout simulation results for V_{EH} .

For schematic simulation a DC voltage close to 307.16 mV is obtained at $C_{EH} = 100 \mu\text{F}$. This implies $\eta_v = 76.79\%$. The time taken by the capacitor to charge up to 307.16 mV is $T_{C_{EH}} = 224.91$ ms. Therefore, 75.7% of the input signal energy has been harvested by using the *eSampling* system. In addition, V_{EH} , $T_{C_{EH}}$, η_v , and η_e have been calculated from post-layout simulations as 304.7 mV, 250.12 ms, 76.175% and around 67%, respectively. The degradation in performance is due to the parasitic capacitance and resistance involved in the post-layout simulations.

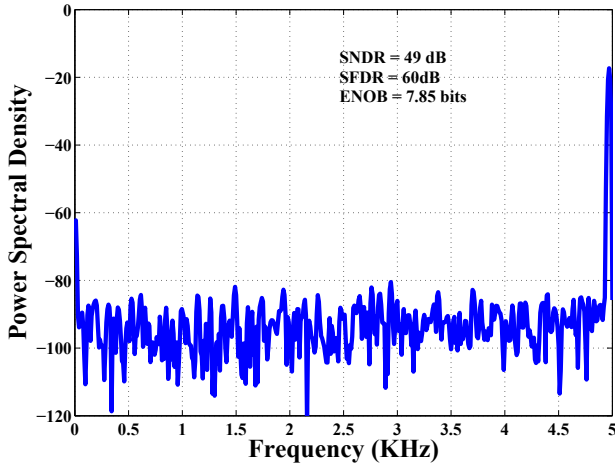


Fig. 6. FFT plot of 8-bit SAR ADC for 10 KHz sampling frequency.

B. High-frequency Simulation of *eSampling* System

In this section, the proposed model is simulated at a sampling frequency of 40 MHz. Following the above specification, the SAR ADC is designed to operate at $T_{aq} = 0.1 T_s = 2.5$ ns with $C_u = 15$ fF. A sinusoidal signal with $V_M = 0.4$ V is considered with the source impedance of 50 Ohm. The obtained input signal rms power (P_{in}) is $27.255 \mu\text{W}$.

From schematic simulations, the output SNDR of $S1$ is around 61 dB. The FFT plot of the reconstructed signal is presented in Fig. 9. From the plot, it is observed that the achievable SNDR and ENOB are 48.52 dB and 7.77 bits, respectively. Furthermore, from post-layout simulations, the obtained output SNDR of $S1$ is around 58 dB, which is greater

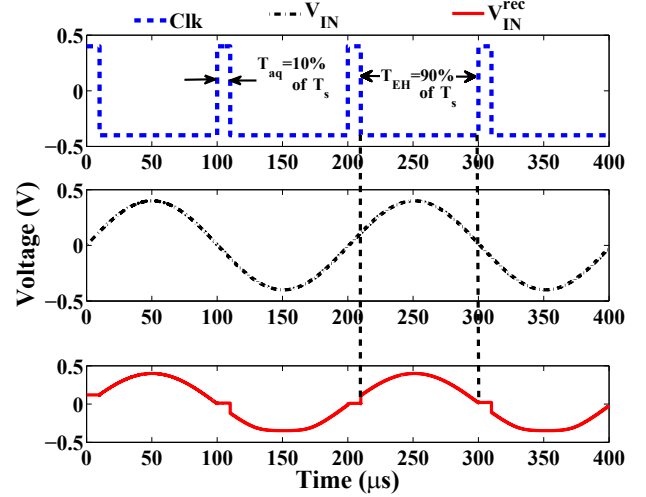


Fig. 7. Sampling clock, input signal and input to the rectifier in the EH branch at 10 KHz sampling frequency.

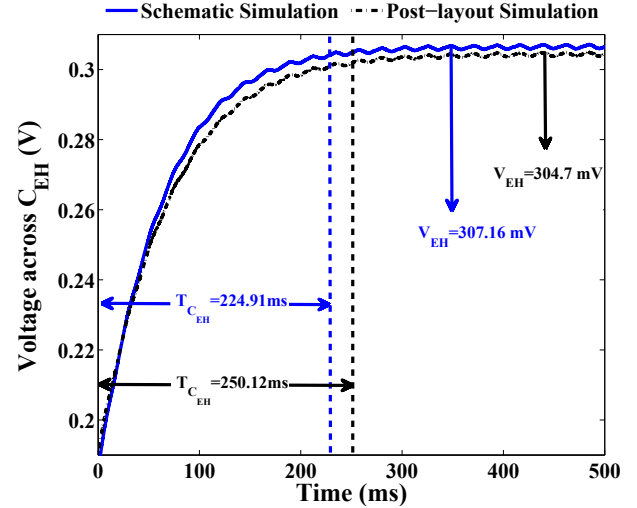


Fig. 8. Voltage obtained across C_{EH} at 10 KHz sampling frequency.

than $6.02n + 1.76$ dB. Therefore, as mentioned above, it can drive an 8-bit SAR ADC.

Simulation results of EH branch is presented in Fig. 10. Compared to the low frequency operation (Fig. 7), less time is available for energy harvesting during the high frequency operation. The obtained V_{in}^{rec} is rectified and stored in C_{EH} as shown in Fig. 11. From schematic simulations, a DC voltage of 304 mV is obtained across $C_{EH} = 25$ nF without degrading the performance of ADC. This implies $\eta_v = 76\%$. The time taken by C_{EH} to charge up to $V_{EH} = 304$ mV is $T_{C_{EH}} = 58.32 \mu\text{s}$. Therefore, 72.64% of the input energy could be harvested using the proposed system model at high frequency. In addition, V_{EH} , $T_{C_{EH}}$, η_v , and η_e have been calculated from post-layout simulations as 300 mV, $63 \mu\text{s}$, 75% and around 65.53%, respectively. The degradation in performance is due to the parasitic capacitance and resistance involved in the post-layout simulations.

TABLE I
PERFORMANCE METRIC

Operation		T_s (μ s)	T_{aq} (μ s)	T_{EH} (μ s)	C_{EH} (μ F)	V_{EH} (mV)	$T_{C_{EH}}$ (ms)	η_v (%)	η_e (%)
Sampling@10 KHz	Schematic	100	10	90	100	307.16	224.91	76.79	75.7
	Post-layout					304.7	250.12	76.175	67
Sampling@40 MHz	Schematic	0.025	0.0025	0.0225	0.025	304	0.05832	76	72.64
	Post-layout					300	0.063	75	65.53

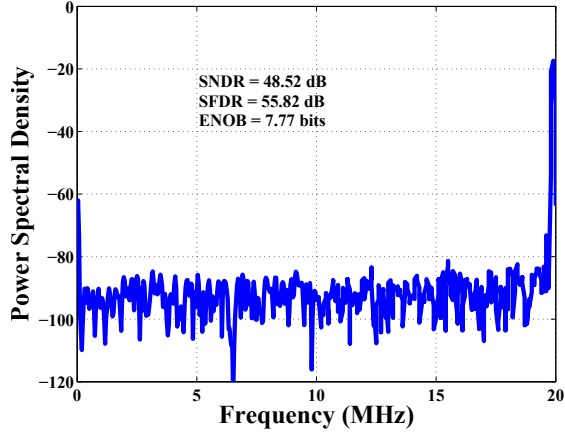


Fig. 9. FFT plot of 8-bit SAR ADC for 40 MHz sampling frequency.

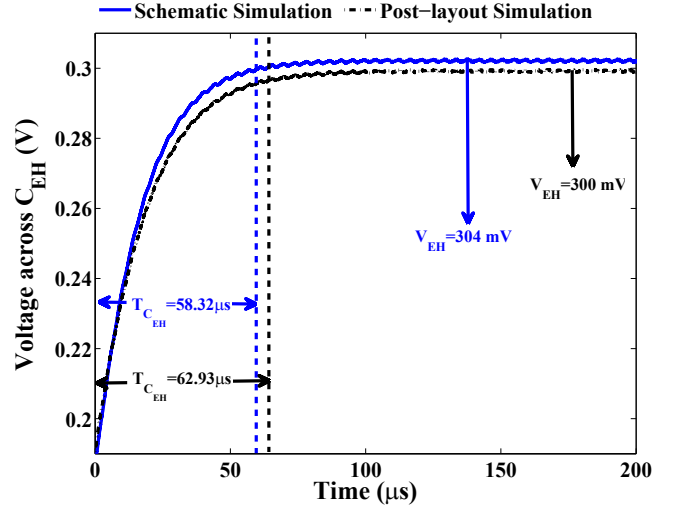


Fig. 11. Voltage obtained across C_{EH} at 45 MHz KHz sampling frequency.

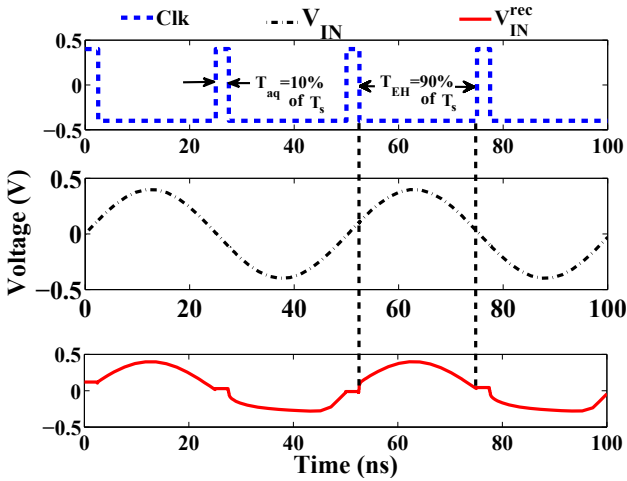


Fig. 10. Sampling clock, input signal and input to the rectifier in the EH branch at 40 MHz.

C. Discussion

For both low and high frequency simulations, it is observed that the input signal energy can be harvested while maintaining the optimal performance of 8 bit SAR ADC ($ENOB \geq 7.75$ bits at the Nyquist rate). The obtained results for high and low frequency simulations are summarized in Table I.

The size of the energy harvesting capacitor, i.e., C_{EH} plays an important role and generally based upon the load to be driven. It can be expressed as

$$C_{EH} = \frac{I_{load} T_p}{\Delta V}, \quad (9)$$

where I_{load} is the load current, T_p is the duration between two consecutive peaks of ripples, and ΔV is the amount of ripple that can be tolerated by the load. From equation (9), it is seen that the small value of ΔV implies large C_{EH} . However, a larger value of C_{EH} implies that more time will be taken by the capacitor to charge up to the peak value. Therefore, the capacitor might not be charged to the maximum input signal amplitude, which implies $\eta_v < 1$ (2). Hence, depending upon the load conditions, a suitable value of C_{EH} should be selected.

Generally, electronic systems have lower ripple tolerance capability, and hence $\Delta V \approx 1$ mV has been considered in this paper. In order to have a fair comparison between low and high frequency setup, C_{EH} for both setup have been calculated under similar load condition, i.e., $\Delta V \approx 1$ mV. The value of C_{EH} obtained for low and high frequency setup is 100 μ F and 25 nF, respectively. It is observed that $\frac{C_{EH}}{T_{C_{EH}}}$ for both setup is around 0.4×10^{-3} F/s. However, the value of V_{EH} is 307.16 mV and 304 mV for low and high frequency, respectively. Therefore, slightly lower conversion efficiency is obtained for high frequency setup under similar load condition. It may be noted that the high frequency setup can also attain $V_{EH} = 307.16$ mV (same as of low frequency) if $C_{EH} = 7$ nF. However, such small value of C_{EH} will provide high amount of ripples ($\Delta V > 7$ mV).

Furthermore, if harvested voltage has to drive an application or load which require supply voltage (V_L) much greater than V_{EH} , then dc-dc converter [40]–[42] can be deployed to boost



Fig. 12. Harvested Voltage boosted to the required level (V_L)

V_{EH} up to V_L in the EH branch as shown in Fig. 12.

V. REAL TIME VALIDATION OF *eSampling*

A. Hardware setup

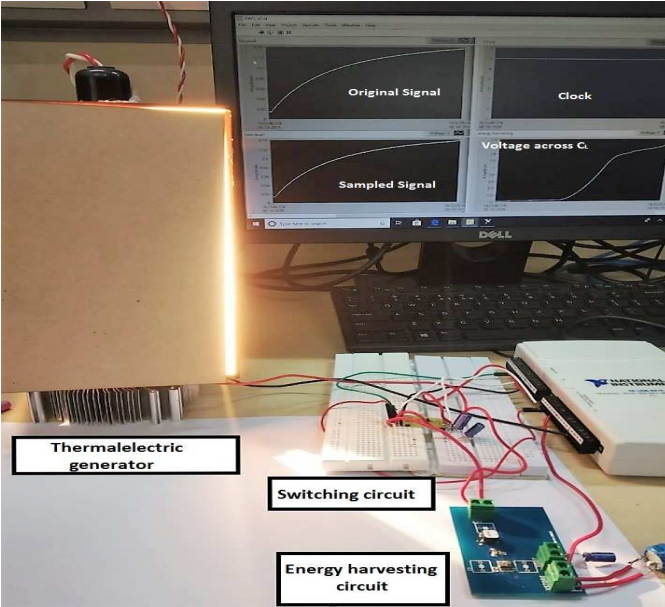


Fig. 13. Hardware Prototype

To demonstrate the proposed *eSampling* framework in real world environment, a hardware set up similar to Fig. 2 a) has been built. The hardware prototype has been shown in Fig. 13. The input analog signal, $V_{in}(t)$ is obtained via the sensing of the external temperature using a sensing element i.e., thermal electric generator (TEG). TEG can produce an output voltage from 10 mV to 50 mV per $^{\circ}\text{C}$ change in temperature [43]. The switches $S1$ and $S2$ have been implemented using single pole double throw (SPDT) ADG791 monolithic CMOS switch. A *Clk* signal similar to the *low-frequency simulation* set up has been generated externally and applied to ADG719. The switch will connect the $V_{in}(t)$ to one output terminal for duration of 10% of the total sampling period (T_s) and to another output terminal with duration of 90% of the total sampling period, respectively. The output terminals obtaining 10% and 90% time of the total sampling period has been connected to C_h for acquiring data samples and C_{EH} for storing energy, respectively. The maximum voltage received at energy storage capacitor i.e., V_{EH} is boosted up to 5V using a dc-dc converter i.e., LTC3108.

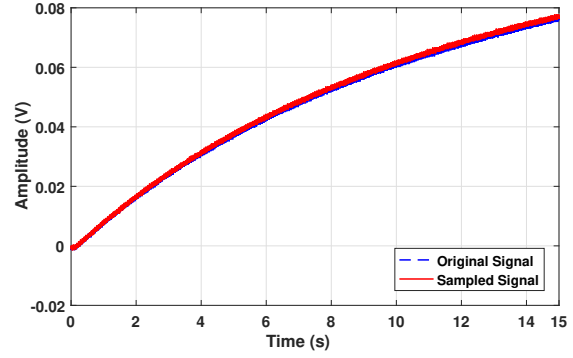


Fig. 14. Voltage obtained across holding capacitor, C_h at 10 KHz sampling frequency in hardware setup .

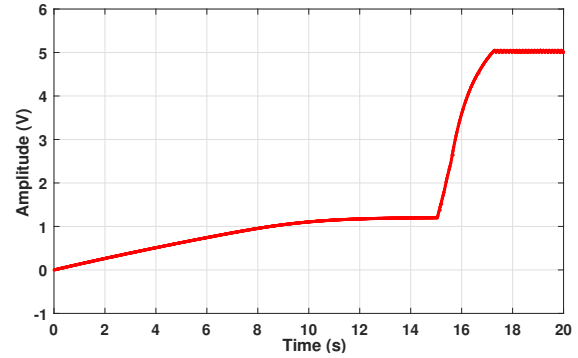


Fig. 15. Voltage obtained across C_L at 10 KHz sampling frequency in hardware setup.

B. Experimental Results

Fig. 14 compares $V_{in}(t)$ with the sampled output voltage obtained at C_h using *eSampling*. From the figure, it can be observed that the input signal is similar to the sampled output signal, and hence harvesting the energy along with sampling using *eSampling* is not degrading the performance of conventional sampling process of an ADC. The experiment has been computed for $f_s = 10 \text{ KHz}$, $T_{aq} = 0.1 T_s$, and hence $T_{EH} = 0.9 T_s$. Furthermore, the harvested voltage has been boosted to $V_L = 5\text{V}$ by using LTC3108 as shown in Fig. 15. The remaining parameters used are as follows: $C_h = 1 \mu\text{F}$, $C_{EH} = 100 \mu\text{F}$ and $C_L = 10 \mu\text{F}$. The time required by C_L to reach 5V is 16.58 seconds as shown in Fig. 15 with conversion efficiency of 64.98%.

VI. CONCLUSION

In this paper, modifications in conventional sampling circuitry of an ADC has been proposed for harvesting energy from the discarded portion of the input analog signal. The method is named as *eSampling*. For validating the presented method, CMOS 65 nm technology based system has been designed. In the experiment, only 10% of the sampling period has been used to sample the signal (with perfect recovery of the original analog signal subsequently), while rest 90% has been used for energy harvesting. The experiment has been performed at both low (10 KHz) as well as high frequency (40 MHz). It is observed that more than 65% conversion

efficiency has been obtained with post-layout simulations for both experiments. The experiment has also been replicated on a hardware set up by obtaining the analog signal from TEG at 10 KHz sampling frequency. The obtained conversion efficiency is 64.98%.

REFERENCES

- [1] T. Hiramoto, K. Takeuchi, T. Mizutani, A. Ueda, T. Saraya, M. Kobayashi, Y. Yamamoto, H. Makiyama, T. Yamashita, H. Oda, S. Kamohara, N. Sugii, and Y. Yamaguchi, "Ultra-low power and ultra-low voltage devices and circuits for IoT applications," in *2016 IEEE Silicon Nanoelectronics Workshop (SNW)*, June 2016, pp. 146–147.
- [2] Keunwoo Kim, R. V. Joshi, and Ching-Te Chuang, "Strained-si devices and circuits for low-power applications," in *Proceedings of the 2003 International Symposium on Low Power Electronics and Design, 2003. ISLPED '03.*, Aug 2003, pp. 180–183.
- [3] J. D. Meindl, "Low power microelectronics: Retrospect and prospect," *Proceedings of the IEEE*, vol. 83, no. 4, pp. 619–635, Apr 1995.
- [4] S. Han, "Moore's law and energy and operations savings in the evolution of optical transport platforms," *IEEE Communications Magazine*, vol. 48, no. 2, pp. 66–69, February 2010.
- [5] S. Fan, R. Wei, L. Zhao, X. Yang, L. Geng, and P. X. . Feng, "An ultralow quiescent current power management system with maximum power point tracking (MPPT) for batteryless wireless sensor applications," *IEEE Transactions on Power Electronics*, vol. 33, no. 9, pp. 7326–7337, Sep. 2018.
- [6] N. Jain and V. A. Bohara, "Energy harvesting and spectrum sharing protocol for wireless sensor networks," *IEEE Wireless Communications Letters*, vol. 4, no. 6, pp. 697–700, Dec 2015.
- [7] X. Lu, P. Wang, D. Niyato, D. I. Kim, and Z. Han, "Wireless networks with RF energy harvesting: A contemporary survey," *IEEE Communications Surveys Tutorials*, vol. 17, no. 2, pp. 757–789, Secondquarter 2015.
- [8] S. Basagni, M. Y. Naderi, C. Petrioli, and D. Spenza, "Wireless sensor networks with energy harvesting," *Mobile Ad Hoc networking: cutting edge directions*, pp. 701–736, 2013.
- [9] A. B. Waluyo, S. Ying, I. Pek, and J. K. Wu, "Middleware for wireless medical body area network," in *2007 IEEE Biomedical Circuits and Systems Conference*, Nov 2007, pp. 183–186.
- [10] H. Yoo and J. Bae, "Low energy wireless body area network systems," in *IEEE International Wireless Symposium (IWS)*, April 2013, pp. 1–2.
- [11] H. Yoo, "Wireless body area network and its healthcare applications," in *2013 Asia-Pacific Microwave Conference Proceedings (APMC)*, Nov 2013, pp. 89–91.
- [12] Y. Rao, K. M. McEachern, and D. P. Arnold, "A compact human-powered energy harvesting system," in *Journal of Physics: Conference Series*, vol. 476, no. 1. IOP Publishing, 2013, p. 012011.
- [13] T. Starmer and J. A. Paradiso, "Human generated power for mobile electronics," *Low-power electronics design*, vol. 45, pp. 1–35, 2004.
- [14] D. Vinnikov, A. Chub, E. Liivik, R. Kosenko, and O. Korkh, "Solar optivertera novel hybrid approach to the photovoltaic module level power electronics," *IEEE Transactions on Industrial Electronics*, vol. 66, no. 5, pp. 3869–3880, May 2019.
- [15] C. Alippi and C. Galperti, "An adaptive system for optimal solar energy harvesting in wireless sensor network nodes," *IEEE Transactions on Circuits and Systems I: Regular Papers*, vol. 55, no. 6, pp. 1742–1750, July 2008.
- [16] L. Zhao, L. Tang, J. Liang, and Y. Yang, "Synergy of wind energy harvesting and synchronized switch harvesting interface circuit," *IEEE/ASME Transactions on Mechatronics*, vol. 22, no. 2, pp. 1093–1103, April 2017.
- [17] G. Verma and V. Sharma, "A novel thermoelectric energy harvester for wireless sensor network application," *IEEE Transactions on Industrial Electronics*, vol. 66, no. 5, pp. 3530–3538, May 2019.
- [18] J. G. Rocha, L. M. Goncalves, P. F. Rocha, M. P. Silva, and S. Lanceros-Mendez, "Energy harvesting from piezoelectric materials fully integrated in footwear," *IEEE Transactions on Industrial Electronics*, vol. 57, no. 3, pp. 813–819, March 2010.
- [19] S. Kim, R. Vyas, J. Bitto, K. Niotaki, A. Collado, A. Georgiadis, and M. M. Tentzeris, "Ambient RF energy-harvesting technologies for self-sustainable standalone wireless sensor platforms," *Proceedings of the IEEE*, vol. 102, no. 11, pp. 1649–1666, Nov 2014.
- [20] R. Zhang and C. K. Ho, "MIMO broadcasting for simultaneous wireless information and power transfer," *IEEE Transactions on Wireless Communications*, vol. 12, no. 5, pp. 1989–2001, May 2013.
- [21] X. Zhou, R. Zhang, and C. K. Ho, "Wireless information and power transfer: Architecture design and rate-energy tradeoff," in *Global Communications Conference (GLOBECOM), 2012 IEEE*, Dec 2012, pp. 3982–3987.
- [22] G. P. Koste, M. Y. Shih, and T. R. Tolliver, "Power harvesting," US Patent US 7,266,269 B2, December, 2004.
- [23] B. Li, W. Xu, S. Li, and J. Lin, "Energy efficient power allocation in OFDM-based CRNs with cyclic prefix power transfer," in *2015 IEEE 81st Vehicular Technology Conference (VTC Spring)*, May 2015, pp. 1–5.
- [24] N. Jain, V. A. Bohara, and A. Gupta, "iDEG: Integrated data and energy gathering framework for practical wireless sensor networks using compressive sensing," *IEEE Sensors Journal*, vol. 19, no. 3, pp. 1040–1051, Feb 2019.
- [25] D. Newell and M. Duffy, "Review of power conversion and energy management for low-power, low-voltage energy harvesting powered wireless sensors," *IEEE Transactions on Power Electronics*, vol. 34, no. 10, pp. 9794–9805, Oct 2019.
- [26] P. Li, Y. Wen, Z. Zhang, and S. Pan, "A high-efficiency management circuit using multiwinding upconversion current transformer for power-line energy harvesting," *IEEE Transactions on Industrial Electronics*, vol. 62, no. 10, pp. 6327–6335, Oct 2015.
- [27] S. S. Gupta and N. B. Mehta, "Revisiting effectiveness of energy conserving opportunistic transmission schemes in energy harvesting wireless sensor networks," *IEEE Transactions on Communications*, vol. 67, no. 4, pp. 2968–2980, April 2019.
- [28] T. D. Nguyen, J. Y. Khan, and D. T. Ngo, "A distributed energy-harvesting-aware routing algorithm for heterogeneous iot networks," *IEEE Transactions on Green Communications and Networking*, vol. 2, no. 4, pp. 1115–1127, Dec 2018.
- [29] F. Akhtar and M. H. Rehmani, "Energy harvesting for self-sustainable wireless body area networks," *IT Professional*, vol. 19, no. 2, pp. 32–40, March 2017.
- [30] M. Vidojkovic, X. Huang, P. Harpe, S. Rampu, C. Zhou, L. Huang, J. van de Molengraft, K. Imamura, B. Busze, F. Bouwens, M. Konijnenburg, J. Santana, A. Breeschoten, J. Huisken, K. Philips, G. Dolmans, and H. de Groot, "A 2.4 GHz ULP OOK single-chip transceiver for healthcare applications," *IEEE Transactions on Biomedical Circuits and Systems*, vol. 5, no. 6, pp. 523–534, Dec 2011.
- [31] P. Harpe, G. Dolmans, K. Philips, and H. de Groot, "A 0.7V 7-to-10bit 0-to-2MS/s flexible SAR ADC for ultra low-power wireless sensor nodes," in *2012 Proceedings of the ESSCIRC*, Sep. 2012, pp. 373–376.
- [32] C. Wulff and T. Ytterdal, "A compiled 3.5fJ/conv.step 9b 20MS/s SAR ADC for wireless applications in 28nm FDSOI," in *ESSCIRC Conference 2016: 42nd European Solid-State Circuits Conference*, Sep. 2016, pp. 177–180.
- [33] R. Atallah, M. Khabbaz, and C. Assi, "Energy harvesting in vehicular networks: a contemporary survey," *IEEE Wireless Communications*, vol. 23, no. 2, pp. 70–77, April 2016.
- [34] V. Hariprasath, J. Guerber, S.-H. Lee, and U.-K. Moon, "Merged capacitor switching based SAR ADC with highest switching energy-efficiency," *Electronics letters*, vol. 46, no. 9, pp. 620–621, 2010.
- [35] B. Razavi, "The bootstrapped switch [a circuit for all seasons]," *IEEE Solid-State Circuits Magazine*, vol. 7, no. 3, pp. 12–15, Summer 2015.
- [36] B. Razavi, *Principles of data conversion system design*. Wiley, 1995, vol. 126.
- [37] H. S. Bindra, C. E. Lokin, D. Schinkel, A. Annema, and B. Nauta, "A 1.2-V dynamic bias latch-type comparator in 65-nm cmos with 0.4-mV input noise," *IEEE Journal of Solid-State Circuits*, vol. 53, no. 7, pp. 1902–1912, July 2018.
- [38] P. J. A. Harpe, C. Zhou, Y. Bi, N. P. van der Meijs, X. Wang, K. Philips, G. Dolmans, and H. de Groot, "A 26μw 8 bit 10 MS/s asynchronous SAR ADC for low energy radios," *IEEE Journal of Solid-State Circuits*, vol. 46, no. 7, pp. 1585–1595, July 2011.
- [39] R. E. Suarez, P. R. Gray, and D. A. Hodges, "All-MOS charge-redistribution analog-to-digital conversion techniques. ii," *IEEE Journal of Solid-State Circuits*, vol. 10, no. 6, pp. 379–385, Dec 1975.
- [40] P. Chen and P. M. Fan, "An 83.4multiple-output based adaptive gate biasing dc-dc converter for thermoelectric energy harvesting," *IEEE Transactions on Circuits and Systems I: Regular Papers*, vol. 62, no. 2, pp. 405–412, Feb 2015.
- [41] M. Saadat and B. Murmann, "A 0.6 v2.4 v input, fully integrated reconfigurable switched-capacitor dc-dc converter for energy harvesting

- sensor tags,” in *2015 IEEE Asian Solid-State Circuits Conference (A-SSCC)*, Nov 2015, pp. 1–4.
- [42] C. Veri, M. Pasca, S. D’Amico, and L. Francioso, “A 40mv start up voltage dc - dc converter for thermoelectric energy harvesting applications,” in *2014 10th Conference on Ph.D. Research in Microelectronics and Electronics (PRIME)*, June 2014, pp. 1–4.
- [43] B. Haug, “Wireless sensor nodes can be powered by temperature gradients; no batteries needed: Harvesting energy from thermoelectric generators,” *Ieee power electronics magazine*, vol. 4, no. 4, pp. 24–32, 2017.